INTERNATIONAL JOURNAL FOR NUMERICAL METHODS IN FLUIDS
Int. J. Numer. Meth. Fluids 2008; **56**:1605–1623
Published online 19 June 2007 in Wiley InterScience (www.interscience.wiley.com). DOI: 10.1002/fld.1551

Numerical simulation of minimum B-jumps at abrupt drops

Nuray Denli Tokyay[‡], A. Burcu Altan-Sakarya[*,†,§] and Elvan Eski

Department of Civil Engineering, Middle East Technical University, 06531 Ankara, Turkey

SUMMARY

A numerical simulation of minimum B-jumps in horizontal rectangular channels having an abrupt drop is given. Gradually varied, steady, supercritical flow is assumed as the initial condition. An unsteady flow is created by increasing the downstream depth. One-dimensional, unsteady Saint-Venant equations are solved by using the MacCormack and the dissipative two–four explicit finite difference schemes. The steady flow solution is obtained by treating the time variable as an iteration parameter and letting the solution converge to the steady state. The abrupt drop is treated as an interior boundary and solved by the method of characteristics. The results are compared with experimental and analytical studies. Copyright © 2007 John Wiley & Sons, Ltd.

Received 27 November 2006; Revised 30 April 2007; Accepted 14 May 2007

KEY WORDS: hydraulic jump; minimum B-jump; abrupt drop; numerical simulation; finite difference scheme

1. INTRODUCTION

The hydraulic jump used for energy dissipation is usually confined partly or entirely to a channel reach that is known as the stilling basin. The bottom of the basin is paved to resist scouring. In practice, the stilling basin is seldom designed to confine the entire length of a free hydraulic jump on the paved apron, because such a basin would be too expensive. Consequently, accessories to control the jump are usually installed in the basin. The main purpose of such control is to shorten the range within which the jump will take place and thus to reduce the size and cost of the stilling basin. The control has additional advantages, for it improves the dissipation function of the basin, stabilizes the jump action and in some cases increases the factor of safety.

In the design of stilling basins, whenever the tailwater depth is greater than the required sequent depth of a simple hydraulic jump, the jump moves upstream and causes drowned jump which

*Correspondence to: A. Burcu Altan-Sakarya, Department of Civil Engineering, Middle East Technical University, 06531 Ankara, Turkey.
†E-mail: burcuas@metu.edu.tr
‡Associate Professor.
§Assistant Professor.

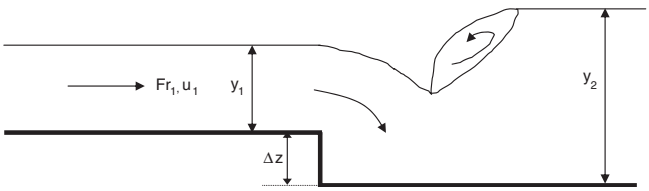

Figure 1. Schematic representation of minimum B-jump.

reduces the efficiency of the structure and the jump. The only way to prevent drown jumps is to use an abrupt drop. But experiments show that, when the jump is controlled by abrupt drops, four different forms of flow occur. The formation of these different types of hydraulic jumps at an abrupt drop depends on the upstream Froude number, the relative depth of tailwater with respect to initial depth and the relative drop height [1, 2].

The flow condition for which the jump occurs in the upstream channel reach and the surface roller entirely forming on the step is called A-jump. Lowering the tailwater elevation, the jump moves downstream. The flow on the drop becomes supercritical and a stationary wave forms on the downstream side of the drop. This is characterized by a nearly horizontal upstream profile and a curved surface jet, and it is called wave case. Further lowering the tailwater elevation will cause the wave to break and form a surface roller such that a jump forms right after the drop. This type is called B-jump. B-jumps are characterized by a downward curved jet at the drop. On the drop face, the pressure distribution is non-hydrostatic and may assume subatmospheric values. The velocities near the channel bottom, in front of the drop, are high. Having high scouring power and being ineffective in dissipation of kinetic energy, B-jump is the most undesired jump type. Whenever an abrupt drop is used to control the jump, it becomes important to determine the location of the jump, especially B jump, so that the channel can be protected. Further lowering the tailwater elevations will cause formation of the so-called minimum B-jump, which is the type of jump that occurs away from the drop. A schematic representation of minimum B-jump is shown in Figure 1. In Figure 1, y_1 and y_2 are the upstream and downstream flow depths, respectively. u_1 is the upstream flow velocity and Δz is the drop height. The parameters which determine the jump type are: the upstream Froude number, $Fr_1 = u_1/\sqrt{gy_1}$, relative downstream depth, $Y = y_2/y_1$, and relative drop height, $S = \Delta z/y_1$.

In the literature, although standing waves which occur in channel transitions in supercritical flows and hydraulic jumps have been studied extensively by experimental techniques [3–7], few studies aims to simulate hydraulic jump with all its properties numerically [8, 9]. On the other hand, over the past 10 years, studies focussing on the numerical simulation of sharp transients have been investigated covering the range from the classical shallow water approach [10–13] to sophisticated investigations assuming non-hydrostatic pressure distributions [14–16]. Most of the time, to evaluate the robustness and accuracy of the numerical technique, simulation of hydraulic jump is used as a test case [17, 18]. In these studies, the type of the jump, its relation to the Froude number and depth ratios, its location are not provided. The main concern is on the numerical technique, and hydraulic jump has been used as a test case only. For example, the work of Reference [14] is concerned with the computation of incompressible, axisymmetric, and full three-dimensional free surface flows. In particular, the circular hydraulic jump is simulated and compared with approximate analytic solutions.

DOI: 10.1002/fld

The numerical solutions of open-channel flows are difficult due to defining the boundary conditions of the free surface and also non-rectangular and unknown geometry. In order to eliminate this difficulty, the open channel flow equations are integrated over the depth; leaving the depth as a dependent variable and eliminating the free surface as a boundary of the solution region. By this averaging process, a two-dimensional problem becomes one dimensional. Since the variable part of the boundary is eliminated, the solution domain becomes fixed.

Finite difference techniques have been used in the simulation of open channel flows [19–24]. Gharangik and Chaudry [9] solved the Boussinesq equations to simulate the formations of a simple hydraulic jump in a rectangular channel having a small bottom slope. They also investigated the importance of Boussinesq term. Their simulations showed that the Boussinesq term have little effect in determining the location of the hydraulic jump. Reference [23] describes the development of a mathematical model which solves the one-dimensional unsteady water flow equations. It is based on the MacCormack second-order explicit scheme. The treatment of the external and internal boundaries has been made by means of the method of characteristics. Their solution simulates the shock formations for supercritical flow. These two papers [9, 23] showed that second-order numerical schemes give satisfactory results for the solution of gradually varied flow equations. An unsteady flow model may be used to obtain steady flow solutions by using time as an iteration parameter. If a shock capturing technique is used, mixed sub and supercritical flows, such as hydraulic jumps may also be simulated. In fact, this study together with Gharangik and Chaudry's [9] study inspired us to simulate minimum B-Jumps at abrupt drops.

In the present study, numerical simulation of minimum B-jump at an abrupt drop is investigated. Although there are much more sophisticated numerical methods on the solution of hydraulic jumps [11–16], the present study focuses on a particular case, namely, 'numerical simulation of minimum B-jumps at abrupt drops' by using a relatively simple method by which the location of the jump can also be determined. In the present study, one-dimensional, unsteady Saint-Venant equations are solved by using the MacCormack and the dissipative two–four explicit finite difference schemes. The steady flow solution is obtained by treating the time variable as an iteration parameter and letting the solution converge to the steady-state flow. The abrupt drop is treated as an interior boundary and solved by using the method of characteristics.

2. GOVERNING EQUATIONS

In the solution of gradually varied flow, one-dimensional unsteady Saint-Venant equations may be used. Including the gravity and friction slope terms, the one-dimensional, unsteady Saint-Venant equations for a prismatic channel may be written in vectorial form as [9]

$$\frac{\partial \mathbf{G}}{\partial t} + \frac{\partial \mathbf{F}}{\partial x} = \mathbf{S} \tag{1}$$

where **G**, **F** and **S** are defined as

$$\mathbf{G} = \begin{bmatrix} y \\ uy \end{bmatrix} \tag{2}$$

DOI: 10.1002/fld

$$\mathbf{F} = \begin{bmatrix} uy \\ u^2 y + \frac{1}{2} g y^2 \end{bmatrix} \tag{3}$$

$$\mathbf{S} = \begin{bmatrix} 0 \\ gy(S_o - S_f) \end{bmatrix} \tag{4}$$

in which x is the distance along the channel bottom, t is the time, u and y are the flow velocity and depth in the x-direction, respectively, g is the gravitational acceleration, S_o is the channel bottom slope, and S_f is the friction slope according to Manning equation:

$$S_f = n^2 \frac{u|u|}{R^{4/3}} \tag{5}$$

where, n is the Manning-roughness coefficient, R is the hydraulic radius, and for wide rectangular channels $R \cong y$.

Therefore, in vectorial form, the first component of Equation (1) gives the continuity equation and the second component gives the momentum equation.

3. NUMERICAL SIMULATION METHOD

In order to simulate the hydraulic jump, Equation (1) is solved numerically. The time derivative term is considered as an iteration parameter and the unsteady flow solution is iterated until a steady state is reached. If a shock capturing technique is used, the jump forms as a part of the solution, and its location is predicted. The calculations are started with the initial conditions defined along the channel. The initial conditions are described by assuming a supercritical flow in the entire channel. Then an unsteady flow is introduced by increasing the downstream depth to a value, which gives a subcritical flow.

The horizontal channel is divided into 'N' sections of equal length, Δx. Therefore if the first node (upstream boundary) number is (1), then the last node (downstream boundary) number is $(N + 1)$. Abrupt drop is placed at the Mth node. The initial flow in the channel and the node numbers are shown in Figure 2.

Two numerical schemes are used for the solution: The MacCormack scheme and the dissipative two–four scheme. The MacCormack scheme is second-order accurate both in space and time.

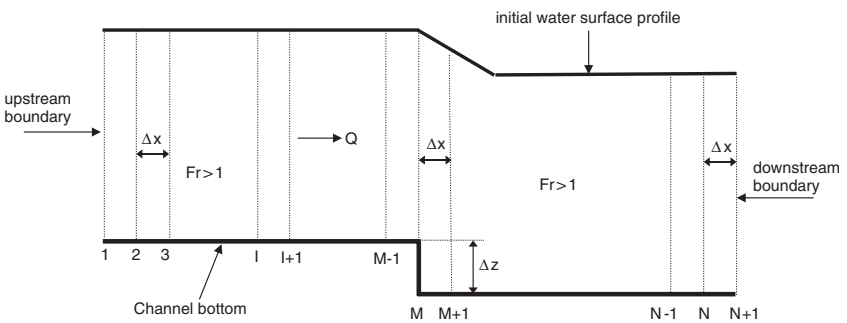

Figure 2. Schematic representation of flow at $t = 0$ (initial condition).

DOI: 10.1002/fld

Dissipative two–four scheme is fourth-order accurate in space and second-order accurate in time. At the computational nodes next to the boundaries, the MacCormack scheme, which requires data only one point upstream and downstream, is used. However, at interior points, where a jump may take place, dissipative two–four scheme, which requires data at two neighbouring nodes is preferred. The abrupt drop is treated as an interior boundary and solved by using the method of characteristics.

3.1. The MacCormack scheme

This scheme is a two-step, non-centred, time-marching explicit finite difference technique developed by MacCormack [25]. It is second-order accurate in space and time. One-sided differences (forward or backward) are used to replace the spatial derivative. The scheme has two steps: predictor and corrector. Forward finite differences are used in the predictor part and backward finite differences in the corrector part. The values of y and u are assumed to be known at time (k) either from the given initial conditions or computed by using the values obtained at the previous time step. Then, the solution at time $(k+1)$ for the computational node (i) is obtained as follows [9]:

Predictor:

$$G_i^* = G_i^k - \lambda(F_{i+1}^k - F_i^k) + \Delta t S_i^k \tag{6}$$

Corrector:

$$G_i^{**} = G_i^* - \lambda(F_i^* - F_{i-1}^*) + \Delta t S_i^* \tag{7}$$

The value of G at time $(k+1)$ is then evaluated as

$$G_i^{k+1} = \tfrac{1}{2}(G_i^k + G_i^{**}) \tag{8}$$

where $\lambda = \Delta t/\Delta x$; k refers to known time level and $(k+1)$ refers to unknown time level. Superscript (*) indicates predicted variable, whereas (**) indicates corrected variable. The subscripts (i), $(i-1)$ and $(i+1)$ refer to computational nodes.

The MacCormack scheme is used to solve the governing equations at the computational nodes which are next to the boundaries, i.e. at the nodes (i) where $i = 2$, $(M-1)$, $(M+2)$, and (N).

Substituting Equations (6) and (7) into (1), the predictor and corrector parts are written as follows.

Predictor:

Continuity equation:

$$y_i^* = y_i^k - \lambda(u_{i+1}^k y_{i+1}^k - u_i^k y_i^k) \tag{9}$$

Momentum equation:

$$\begin{aligned} u_i^* y_i^* = {} & u_i^k y_i^k - \lambda\{[(u_{i+1}^k)^2 y_{i+1}^k + \tfrac{1}{2} g (y_{i+1}^k)^2] - [(u_i^k)^2 y_i^k + \tfrac{1}{2}(g(y_i^k)^2)]\} \\ & + \Delta t g y_i^k (S_o - S_f)_i^k \end{aligned} \tag{10}$$

where

$$S_{fi}^k = \frac{n^2 u_i^k |u_i^k|}{(y_i^k)^{4/3}} \tag{11}$$

DOI: 10.1002/fld

Corrector:

Continuity equation:

$$y_i^{**} = y_i^* - \lambda(u_i^* y_i^* - u_{i-1}^* y_{i-1}^*) \tag{12}$$

Momentum equation:

$$u_i^{**} y_i^{**} = u_i^* y_i^* - \lambda\{[(u_i^*)^2 y_i^* + \tfrac{1}{2} g (y_i^*)^2] - [(u_{i-1}^*)^2 y_{i-1}^* + \tfrac{1}{2} g (y_{i-1}^*)^2]\} + \Delta t g y_i^* (S_o - S_f)_i^* \tag{13}$$

where

$$S_{fi}^* = \frac{n^2 u_i^* |u_i^*|}{(y_i^*)^{4/3}} \tag{14}$$

3.2. Dissipative two–four scheme

This is a finite difference scheme similar to the MacCormack scheme. The scheme was developed by Gottlieb and Turkel [26]. It is a two-step explicit scheme, which is second-order accurate in time and fourth-order accurate in space. The predictor and corrector parts are written as follows.

Predictor:

$$G_i^* = G_i^k + \frac{\lambda}{6}(F_{i+2}^k - 8F_{i+1}^k + 7F_i^k) + \Delta t S_i^k \tag{15}$$

Corrector:

$$G_i^{**} = G_i^* + \frac{\lambda}{6}(-7F_i^* + 8F_{i-1}^* - F_{i-2}^*) + \Delta t S_i^* \tag{16}$$

Therefore, the solution of G at the ith node at time $(k+1)$ is the average of the predictor and corrector:

$$G_i^{k+1} = \tfrac{1}{2}(G_i^k + G_i^{**}) \tag{17}$$

When Equations (15) and (16) are substituted into (1), continuity and momentum equations can be expressed as follows.

Predictor:

Continuity equation:

$$y_i^* = y_i^k + \frac{\lambda}{6}(u_{i+2}^k y_{i+2}^k - 8u_{i+1}^k y_{i+1}^k + 7u_i^k y_i^k) \tag{18}$$

Momentum equation:

$$u_i^* y_i^* = u_i^k y_i^k + \frac{\lambda}{6}\left\{\left[(u_{i+2}^k)^2 y_{i+2}^k + \frac{1}{2} g (y_{i+2}^k)^2\right] - 8\left[(u_{i+1}^k)^2 y_{i+1}^k + \frac{1}{2} g (y_{i+1}^k)\right] + 7\left[(u_i^k)^2 y_i^k + \frac{1}{2} g (y_i^k)^2\right]\right\} + \Delta t g y_i^k (S_o - S_f)_i^k \tag{19}$$

DOI: 10.1002/fld

in which

$$S_{fi}^{k} = \frac{n^2 u_i^k |u_i^k|}{(y_i^k)^{4/3}} \tag{20}$$

Corrector:

Continuity equation:

$$y_i^{**} = y_i^* + \frac{\lambda}{6}(-7u_i^* y_i^* + 8u_{i-1}^* y_{i-1}^* - u_{i-2}^* y_{i-2}^*) \tag{21}$$

Momentum equation:

$$u_i^{**} y_i^{**} = u_i^* y_i^* + \frac{\lambda}{6}\left\{-7\left[(u_i^*)^2 y_i^* + \frac{1}{2}g(y_i^*)^2\right] + 8\left[(u_{i-1}^*)^2 y_{i-1}^* + \frac{1}{2}g(y_{i-1}^*)^2\right] - \left[(u_{i-2}^*)^2 y_{i-2}^* + \frac{1}{2}g(y_{i-2}^*)^2\right]\right\} + \Delta t g y_i^*(S_o - S_f)_i^* \tag{22}$$

in which

$$S_{fi}^{*} = \frac{n^2 u_i^* |u_i^*|}{(y_i^*)^{4/3}} \tag{23}$$

The dissipative two–four scheme can be used at the interior computational nodes, where the values of variables at two neighbouring nodes are required, that is at the nodes $i = 3, 4, \ldots, (M-3)$, $(M-2)$, $(M+3)$, $(M+4)$, $\ldots$, $(N-2)$, $(N-1)$.

3.3. Initial condition

As an initial condition, flow depth and velocity at every computational node should be defined at time $t = 0$. The flow is assumed to be supercritical in the channel initially and the water surface profile is determined by numerical integration of the gradually varied flow equation for wide rectangular channels [27]:

$$L = \frac{y_c^{4/3}}{gn^2}\left[\frac{3}{4}\left(\frac{y}{y_c}\right)^{4/3} - \frac{3}{13}\left(\frac{y}{y_c}\right)^{13/3}\right] + C \tag{24}$$

where L is the distance along channel in the flow direction, y_c is the critical flow depth, and C is the constant of integration.

From Equation (24), the distance, ΔL, between any two successive sections can be written as

$$\Delta L = \frac{y_c^{4/3}}{gn^2}\left\{\frac{3}{4}\left[\left(\frac{y_i}{y_c}\right)^{4/3} - \left(\frac{y_{i-1}}{y_c}\right)^{4/3}\right] - \frac{3}{13}\left[\left(\frac{y_i}{y_c}\right)^{13/3} - \left(\frac{y_{i-1}}{y_c}\right)^{13/3}\right]\right\} \tag{25}$$

Equation (25) can be solved for y_i/y_c by iteration as

$$\frac{y_i}{y_c} = \left\{\frac{4}{3}\left[A + \frac{3}{13}\left(\frac{y_i}{y_c}\right)^{13/3}\right]\right\}^{3/4} \tag{26}$$

DOI: 10.1002/fld

where

$$A = \frac{gn^2}{y_c^{4/3}}\Delta x + \frac{3}{4}\left(\frac{y_{i-1}}{y_c}\right)^{4/3} - \frac{3}{13}\left(\frac{y_{i-1}}{y_c}\right)^{13/3} \tag{27}$$

By assuming the flow depth and velocity at the first section ($i = 1$), the depths at other sections can be determined iteratively from Equation (26), for $i = 2, 3, \ldots, M, M + 2, \ldots, N, N + 1$. For node $(M + 1)$, the initial flow depth is calculated by solving the continuity and energy equations simultaneously.

Continuity equation:

$$u_M y_M = u_{M+1} y_{M+1} \tag{28}$$

Energy equation:

$$y_M + (1 + \eta)\frac{u_M^2}{2g} + \Delta z = y_{M+1} + \frac{u_{M+1}^2}{2g} \tag{29}$$

where η is the minor loss coefficient due to abrupt drop.

3.4. Boundary conditions

The MacCormack and the dissipative two–four scheme can be used for interior nodes but not on the boundary nodes. This is because there are grid points only on one side of the boundary. Therefore, conditions imposed by the boundary should be either specified or determined by a suitable technique. Proper care has to be taken so that the boundary conditions are neither under-specified nor over-specified [20].

The boundary condition that should be specified depends on the flow regime. If the flow is supercritical, two conditions should be specified at the upstream boundary and none at the downstream boundary. If it is subcritical, one condition at the upstream boundary and one condition at the downstream boundary should be specified. As stated by Garcia-Navarro and Saviron [23], other variable can be found by using the method of characteristics.

The boundary contains an abrupt drop at node M. The discontinuity introduced by the drop is eliminated by treating the drop as an internal boundary. The MacCormack and the dissipative two–four schemes described in previous section are used to determine the flow depths and velocities at interior computational nodes. To compute the flow conditions at internal and downstream boundaries, the standard method of characteristics is used [28].

3.4.1. Upstream boundary. At the upstream boundary, the flow is supercritical and the flow conditions do not change during the solution. Therefore, two conditions, flow depth and flow velocity are specified at the first computational node, $i = 1$. These two values remain unchanged at each time level.

3.4.2. Downstream boundary. At the downstream boundary, the flow is subcritical. Therefore, one condition is specified and the other variable is computed by the method of characteristics. At $(N + 1)$th node, a constant flow depth is given. The velocity can be found from the positive characteristic equation [28]. The computational grid is shown in Figure 3. In Figure 3, nodes A and C correspond to nodes (N) and $(N + 1)$, respectively. Here in only the equations used will

DOI: 10.1002/fld

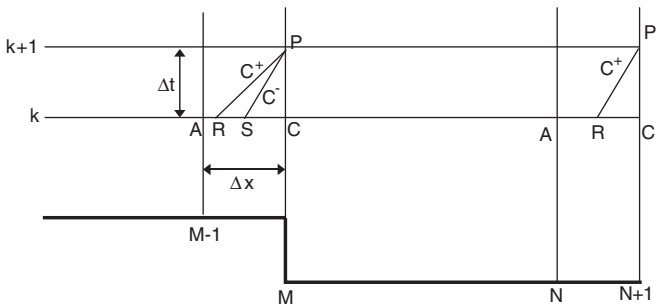

Figure 3. Notation for characteristic curves at downstream and interior boundaries.

be given. The notation for the positive (C^+) and negative (C^-) characteristics equations is given in Figure 3.

Using this notation and $\lambda = \Delta t/\Delta x$, the method of characteristics gives the velocity at point R as

$$u_R = \frac{u_C + \lambda(c_C u_A - c_A u_C)}{1 + \lambda(u_C - u_A + c_C - c_A)} \tag{30}$$

in which $c = \sqrt{gy}$ is the celerity of a small amplitude gravity wave in a rectangular channel for shallow water. Then, the celerity and the depth at point R are, respectively

$$c_R = \frac{c_C + \lambda u_R(c_C - c_A)}{1 + \lambda(c_C - c_A)} \tag{31}$$

$$y_R = y_C - \lambda(u_R + c_R)(y_C - y_A) \tag{32}$$

After having obtained the values at point R, the velocity at point P can be computed. As stated before, point P corresponds to the new time level of node $(N+1)$. Substituting the notation used in the finite difference schemes, the velocity at node $(N+1)$ at time level $(k+1)$ can be expressed as follows:

$$u_{N+1}^{k+1} = u_R^k - \frac{g}{c_R^k}(y_{N+1}^{k+1} - y_R^k) - g\Delta t(S_{f_R} - S_o)^k \tag{33}$$

3.4.3. Interior boundary. Saint-Venant equations are not valid at the abrupt drop since a discontinuity occurs in the flow. Therefore, the drop should be treated as an interior boundary and solved by other techniques. Node (M) can be considered as a downstream boundary to the first reach of the channel and node $(M+1)$ can be considered as an upstream boundary to the second reach. The unknowns at these nodes are the depths of flow, y_M and y_{M+1}, and the velocities, u_M and u_{M+1} at time level $(k+1)$. In case of minimum B-jump, the flow will be supercritical on the drop. For supercritical flow, both C^+ and C^- characteristic lines proceed in the flow direction. Therefore, C^+ and C^- characteristic equations can be both used for node (M). Two of the four unknowns, y_M and u_M can be solved by these two equations. After obtaining two unknowns, remaining two unknowns, y_{M+1} and u_{M+1} can be solved by using the continuity and the energy equations. Since minimum B-jump occurs after the drop, the frictional head loss is negligible and energy equation can be written between sections (M) and $(M+1)$ by using a minor loss coefficient due to the drop.

DOI: 10.1002/fld

The notation for the characteristic equations used for the supercritical flow on the drop, i.e. at (M)th node, is shown in Figure 3. Here, nodes A and C denote nodes $(M-1)$ and (M), respectively.

For computing the values of variables at point R, the method of characteristics are used. The velocity, celerity and the flow depth at point R are calculated by using the Equations (30)–(32).

The variables at point S can be calculated as

$$u_S = \frac{u_C - \lambda(c_C u_A - c_A u_C)}{1 + \lambda(u_C - u_A - c_C + c_A)} \tag{34}$$

$$c_S = \frac{c_C - \lambda u_S(c_C - c_A)}{1 - \lambda(c_C - c_A)} \tag{35}$$

$$y_S = y_C - \lambda(u_S - c_S)(y_C - y_A) \tag{36}$$

With the variables determined at points R and S, the depth y, and the velocity u at node (M) at time level $(k+1)$ can be determined, respectively as

$$y_P = y_M^{k+1} = \frac{1}{(c_R + c_S)^k}\left\{ y_S c_R + y_R c_S + c_R c_S \left[\frac{u_R - u_S}{g} - \Delta t(S_{f_R} - S_{f_S}) \right] \right\}^k \tag{37}$$

$$u_P = u_M^{k+1} = u_R^k - \frac{g}{c_R^k}(y_M^{k+1} - y_R^k) - g\Delta t(S_{f_k} - S_o)^k \tag{38}$$

After obtaining the values of y_M^{k+1} and u_M^{k+1} the values of y_{M+1}^{k+1} and u_{M+1}^{k+1} can be obtained by solving equations of continuity and energy simultaneously as follows:

Continuity:

$$u_M^{k+1} y_M^{k+1} = u_{M+1}^{k+1} y_{M+1}^{k+1} \tag{39}$$

Energy:

$$y_M^{k+1} + \frac{(u_M^{k+1})^2}{2g}(1+\eta) + \Delta z = y_{M+1}^{k+1} + \frac{(u_{M+1}^{k+1})^2}{2g} \tag{40}$$

where η is the minor loss coefficient due to abrupt drop.

3.5. Stability condition

In order the MacCormack and the dissipative two–four schemes to be stable, a limitation on time-step size, Δt should be imposed. Both schemes are stable if Courant–Friedrichs–Lewy (CFL) criterion is satisfied. This criterion is expressed by the following equation [9]:

$$\Delta t = c_n \frac{\Delta x}{\max(|u| + \sqrt{gy})} \tag{41}$$

where c_n is the Courant number. This condition should be satisfied at each iteration level for all grid points. Hence, a minimum time step, which is the same at all grid points but varies from one time step to another is used. For the MacCormack scheme c_n must be less than or equal to 1, whereas for the dissipative two–four scheme, c_n must be less than or equal to $\frac{2}{3}$ [26]. In the present study c_n is chosen as 0.65 in order to satisfy both schemes.

DOI: 10.1002/fld

The grid length should be small enough to locate the jump accurately, while it should be big enough to allow the solution in a reasonable computer time. The computational grid length Δx is chosen as 0.05 m by using several trials.

3.6. Artificial viscosity

The MacCormack and the dissipative two–four schemes produce dispersive errors. These dispersive errors cause high frequency oscillations near steep gradients. To dampen the high frequency oscillations near the steep gradients, a procedure called artificial viscosity is used [22]. This artificial viscosity method dampens the oscillations that are near steep gradients but leaves smooth regions undisturbed.

The variables computed at each time step is modified as follows. First, a parameter ξ_i is computed from one of the variables. In this study, the unit discharge (uy) is used.

$$\xi_i = \left| \frac{u_{i+1}y_{i+1} - 2u_i y_i + u_{i-1}y_{i-1}}{|u_{i+1}y_{i+1}| + 2|u_i y_i| + |u_{i-1}y_{i-1}|} \right| \tag{42}$$

$$\xi_{i+(1/2)} = \kappa \frac{\Delta x}{\Delta t} \max(\xi_{i+1}, \xi_i) \tag{43}$$

$$\xi_{i-(1/2)} = \kappa \frac{\Delta x}{\Delta t} \max(\xi_i, \xi_{i-1}) \tag{44}$$

where κ is the dissipation constant.

The computed variables at new time level are then corrected by using the following equation:

$$f_i^{k+1} = f_i^{k+1} + \xi_{i+(1/2)}(f_{i+1}^{k+1} - f_i^{k+1}) - \xi_{i-(1/2)}(f_i^{k+1} - f_{i-1}^{k+1}) \tag{45}$$

where f is any parameter evaluated by numerical method, and κ indicates the amount of dissipation. Its value should be as low as possible while still dampening high frequency oscillations. Typical values of κ can vary between 0.01 and 0.6. In the present study, the value of κ is determined by trial and error and is taken as 0.11.

4. NUMERICAL RESULTS AND DISCUSSION

4.1. Test of numerical method

The numerical method is tested with the data given in Table I, in which the data for q and Δz are taken from Gür [29] for test numbers 1–10, and the data for test numbers 11–14 are assumed values. The flow depths at upstream and downstream boundaries, y_{us} and y_{ds}, respectively, are estimated from the data of Gür [29] as the water surface profiles in the channel are not given. The following values are used in the computations: $n = 0.008$, $\eta = 0.1$, $\kappa = 0.11$ and $c_n = 0.65$, and $\Delta x = 0.05$ m.

The variable time step Δt is computed from Equation (41) for the fixed Δx and c_n values at each time step within the program. The initial steady-state depth and velocity at every node is computed by using the prescribed upstream depth y_{us}, unit discharge q and step height Δz. Then the unsteady computations are started by increasing the downstream depth to y_{ds} and continued

DOI: 10.1002/fld

Table I. Experimental test conditions.

Test no.	y_{us} (m)	y_{ds} (m)	q (m^2/s)	Δz (m)
1	0.0292	0.0930	0.0420	0.030
2	0.0370	0.1470	0.0732	0.040
3	0.0247	0.1122	0.0470	0.030
4	0.0267	0.1302	0.0552	0.040
5	0.0206	0.1150	0.0420	0.063
6	0.0179	0.0993	0.0360	0.030
7	0.0140	0.0856	0.0280	0.040
8	0.0154	0.1025	0.0352	0.030
9	0.0179	0.1210	0.0450	0.030
10	0.0193	0.1500	0.0554	0.040
11	0.0179	0.1210	0.0450	0.034
12	0.0193	0.1500	0.0554	0.072
13	0.0188	0.1500	0.0554	0.051
14	0.0179	0.0993	0.0360	0.040

Table II. Results of numerical simulation.

Test no.	y_1 (m)	y_2 (m)	Fr_1	S	Y
1	0.0316	0.0946	2.39	0.95	2.99
2	0.0391	0.1480	3.02	1.02	3.79
3	0.0270	0.1132	3.38	1.11	4.19
4	0.0289	0.1310	3.59	1.38	4.53
5	0.0230	0.1157	3.84	2.74	5.03
6	0.0204	0.1002	3.94	1.47	4.91
7	0.0166	0.0864	4.18	2.41	5.20
8	0.0180	0.1032	4.65	1.67	5.73
9	0.0203	0.1216	4.97	1.48	5.99
10	0.0217	0.1505	5.53	1.84	6.94
11	0.0203	0.1216	4.97	1.67	5.99
12	0.0217	0.1505	5.53	3.32	6.94
13	0.0212	0.1505	5.73	2.41	7.10
14	0.0204	0.1001	3.94	1.96	4.91

until the steady-state conditions are reached. Steady-state condition is checked by the maximum relative error, e_{max}, defined as

$$e_{max} = \left| \frac{y_i^{k+1} - y_i^k}{y_i^k} \right| < \text{tolerance} \tag{46}$$

Hence, the maximum relative error between current and previous water depths over the channel should be less than a tolerance defined. Normally, tolerance was set to 0.5×10^{-4} [30]. However, for some test runs, it is seen that the solution converged with some oscillations which is also stated to be a well-known behaviour of the MacCormack scheme [30]. Hence, the number of iteration used is set to 10 000, which only takes couple of minutes to run. It should be noted that in all test runs, the maximum relative error is less than 5×10^{-4} and each test case reached steady state at a different time due to the variable time increment, Δt.

DOI: 10.1002/fld

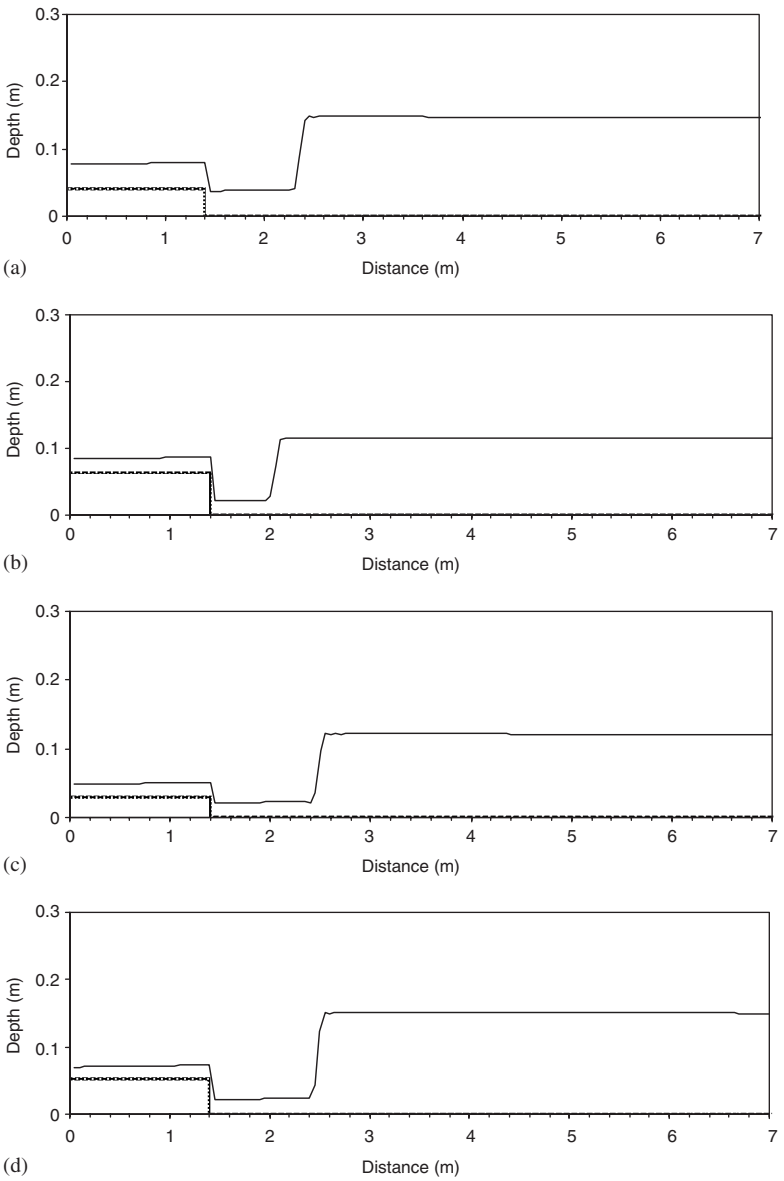

Figure 4. Hydraulic jump profiles: (a) test number (2); (b) test number (5); (c) test number (9); and (d) test number (13).

The results are shown in Table II, in which y_1 is the depth on step, which is assumed to be the initial depth of the jump, y_2 is the final depth of the jump, $Fr_1 = u_1/\sqrt{gy_1}$ is the Froude number of upstream flow, $S = \Delta z/y_1$ is the relative step height, and $Y = y_2/y_1$ is the depth ratio. For the data used, the ranges of Froude number and relative step height are as follows: $2.39 \leqslant Fr_1 \leqslant 5.37$ and $0.95 \leqslant S \leqslant 3.32$.

DOI: 10.1002/fld

The jump profiles computed for test numbers 2, 5, 9 and 13 are shown in Figure 4, which shows that the numerical model is capable of computing the profile of minimum B-jumps at an abrupt drop.

4.2. Verification of numerical method

For the hydraulic jump at an abrupt drop the depth ratio, $Y = y_2/y_1$ depends on the upstream Froude number and the relative step height, i.e. $Y = F(Fr_1, S)$. Test conditions are compared with the closest measured values of Y, Fr_1 and S, in Table III with the available data in the literature. Note that the numerically computed and experimentally obtained values of Fr_1 and S are not exactly the same, but very close to each other.

Since $Y = F(Fr_1, S)$, it is expected that the depth ratio computed must be close to the measured values. The percent error between computed and measured values is defined as

$$e_1 = \left| \frac{Y_{\text{measured}} - Y_{\text{computed}}}{Y_{\text{measured}}} \right| \times 100 \tag{47}$$

It is seen from Table III that the maximum error is 9.31%.

The analytical solutions in the literature give only the relation between Fr_1, Y and S, but not the location of the jump. These relations are as follows:

Moore and Morgan [2]:

$$Fr_1^2 = \frac{Y - (1 + S^2)}{2(1 - 1/Y)} \tag{48}$$

Hager [5]:

$$Fr_1^2 = \frac{Y^2 - S^2 - 1}{2(1 - 1/Y)} \tag{49}$$

Table III. Comparison of numerical prediction with measured values.

	Numerical results			Experimental results				
Test no.	Fr_1	S	Y	Fr_1	S	Y	Error, e_1 %	Source
2	3.02	1.02	3.79	3.00	1.00	3.85	1.68	Ohtsu and Yasuda [7]
3	3.38	1.11	4.19	3.38	1.06	4.34	3.40	Gür [29]
4	3.59	1.38	4.53	3.60	1.34	4.54	0.16	Gür [29]
5	3.84	2.74	5.03	3.72	2.74	5.11	1.56	Gür [29]
6	3.94	1.47	4.91	3.98	1.4	4.82	1.90	Gür [29]
8	4.65	1.67	5.73	4.64	1.68	5.37	6.77	Gür [29]
9	4.97	1.48	5.99	4.92	1.48	5.48	9.31	Gür [29]
11	4.97	1.67	5.99	4.93	1.67	6.13	2.28	Hager and Bretz [31]
12	5.53	3.32	6.94	5.49	3.3	6.91	0.37	Hager and Bretz [31]
13	5.73	2.41	7.10	5.71	2.41	6.98	1.71	Hager and Bretz [31]
14	3.94	1.96	4.91	4.00	2.00	5.40	9.13	Moore and Morgan [2]

DOI: 10.1002/fld

Table IV. Comparison of numerical and analytical predictions.

			Numerical prediction	Analytical prediction from							
				Equation (48)		Equation (49)		Equation (50)		Equation (51)	
Test no.	Fr_1	S	Y	Y	e_2 %	Y	e_2 %	Y	e_2 %	Y	e_2 %
1	2.39	0.95	2.99	3.45	13.19	3.10	3.50	3.29	9.05	2.91	2.78
2	3.02	1.02	3.79	4.25	10.95	3.96	4.50	4.11	7.85	3.80	0.50
3	3.38	1.11	4.19	4.75	11.64	4.47	6.25	4.60	8.78	4.31	2.71
4	3.59	1.38	4.53	5.14	11.80	4.83	6.14	4.93	8.01	4.60	1.41
5	3.84	2.74	5.03	6.23	19.23	5.74	12.31	5.54	9.21	4.96	1.43
6	3.94	1.47	4.91	5.63	12.76	5.33	7.91	5.41	9.28	5.10	3.71
7	4.18	2.41	5.20	6.41	18.83	5.99	13.15	5.90	11.82	5.43	4.19
8	4.65	1.67	5.73	6.62	13.46	6.35	9.65	6.39	10.32	6.10	6.02
9	4.97	1.48	5.99	6.96	13.89	6.72	10.90	6.78	11.71	6.54	8.45
10	5.53	1.84	6.94	7.84	11.57	7.59	8.59	7.61	8.83	7.34	5.53
11	4.97	1.67	5.99	7.03	14.85	6.77	11.55	6.82	12.12	6.54	8.45
12	5.53	3.32	6.94	8.53	18.66	8.10	14.43	7.81	11.22	7.34	5.53
13	5.73	2.41	7.10	8.33	14.78	8.02	11.45	7.95	10.72	7.62	6.83
14	3.94	1.96	4.91	5.88	16.58	5.51	10.88	5.51	11.00	5.10	3.81

Table V. Experimental test conditions.

Test no.	y_{us} (m)	y_{ds} (m)	Δz (m)	q (m^2/s)	Jump occurs at (m)
15	0.0245	0.1020	0.040	0.0410	2.00
16	0.0230	0.1020	0.040	0.0410	2.40
17	0.0200	0.1020	0.040	0.0410	3.30
18	0.0245	0.0980	0.040	0.0410	2.60
19	0.0245	0.0950	0.040	0.0410	3.20
20	0.0245	0.1020	0.050	0.0410	2.30
21	0.0245	0.1020	0.060	0.0410	2.65
22	0.0245	0.1020	0.040	0.0430	2.70
23	0.0245	0.1020	0.040	0.0450	3.55

Tokyay and Gür [6]:

$$Fr_1^2 = \frac{Y^2 - 2S - 1}{2(1 - 1/Y)} \tag{50}$$

Hager and Bretz [31]:

$$Fr_1^2 = \frac{Y(Y+1)}{2} = \frac{Y^2 - 1}{2(1 - 1/Y)} \tag{51}$$

The test results are also compared with the above analytical expressions in Table IV. In Table IV, the relative depth ratio is computed by using Equations (48)–(51) for the given values of Fr_1

DOI: 10.1002/fld

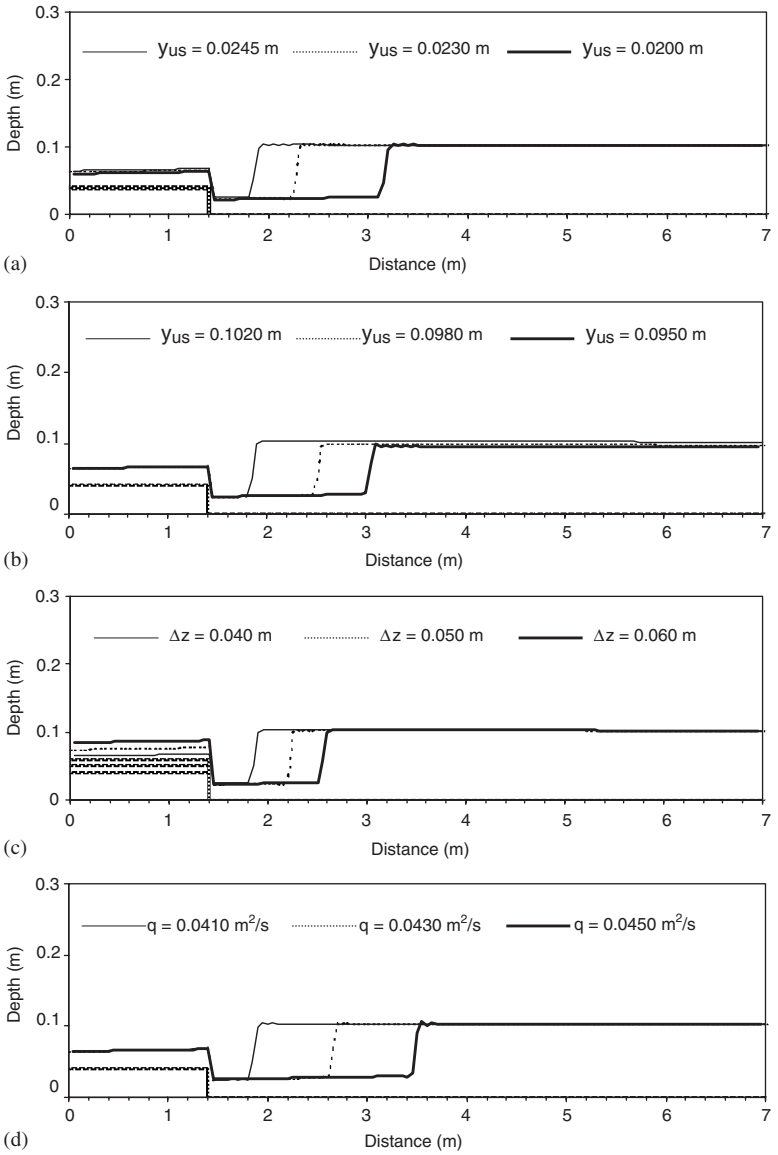

Figure 5. Effect of change in initial data on jump: (a) test numbers (15)–(16)–(17); (b) test numbers (15)–(18)–(19); (c) test numbers (15)–(20)–(21); and (d) test numbers (15)–(22)–(23).

and S. The percent error in Table IV is computed as

$$e_2 = \left| \frac{Y_{\text{analytical}} - Y_{\text{numerical}}}{Y_{\text{analytical}}} \right| \times 100 \tag{52}$$

As can be seen from Table IV, Equation (51) given by Hager and Bretz [31] gives the closest results to the numerical computation. However, this equation is nothing but the equation for a

DOI: 10.1002/fld

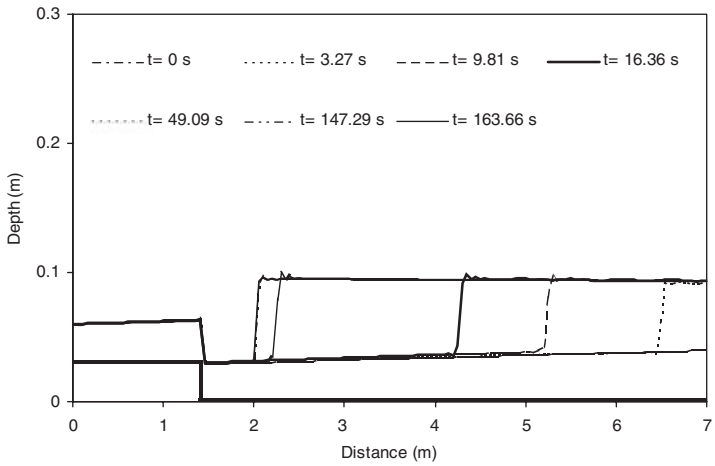

Figure 6. Water surface profiles at different times for test number (1).

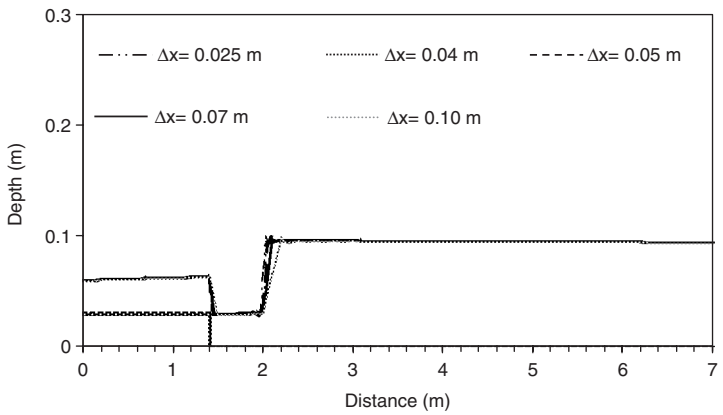

Figure 7. Hydraulic jump profiles obtained using different Δx values for test number (1).

simple hydraulic jump. Hager and Bretz [31] also states that the step height does not affect the jump formation and Equation (51) can be used for the minimum B-jumps at an abrupt drop.

The effect of changing initial data is also tested. The test conditions are shown in Table V in which test number (15) is used as reference data. First the effect of change in upstream depth is tested. For test numbers (16) and (17), the upstream depth is decreased. As it is expected the jump moved downstream as shown in Figure 5(a). The effect of downstream depth is tested in test numbers (18) and (19). In these tests, the downstream depth is decreased, which caused in the jump to move downstream as expected (Figure 5(b)). The effect of step height is tested in test numbers (20) and (21). As step height increased, the jump moved downstream (Figure 5(c)). The effect of increasing unit discharge is tested in test numbers (22) and (23). As the unit discharge increased, the jump moved downstream (Figure 5(d)). The water surface profiles at different times are shown in Figure 6 for test number (1). It is seen that the jump travels upstream until it is

DOI: 10.1002/fld

stabilized. In order to confirm the mesh converged solution of the hydraulic jump, the program is run with different values of Δx, ranging from 0.025 to 0.10 m for test number (1). It can be seen form Figure 7 that the hydraulic jump profiles obtained for different Δx values are very similar to each other. All these tests verify the numerical simulation of a minimum B-jump at an abrupt drop.

5. CONCLUSIONS

The minimum B-jump at an abrupt drop is an example of mixed supercritical and subcritical flow with a discontinuity at the channel bed. The results have shown that the proposed numerical model can handle such flows.

In the numerical model presented, a steady-state flow in a prismatic channel, which has a transition in the form of an abrupt drop, is simulated by using the unsteady flow equations with time variable as an iteration parameter. The results of the numerical model compare well with the analytical results obtained by the one-dimensional, steady flow model and with the observations for a range of $2.39 \leqslant Fr_1 \leqslant 5.73$ for the approach Froude number and $0.95 \leqslant S \leqslant 3.32$ for the relative step height.

The method yields the initial and the sequent depths of the jump for the given upstream and downstream flow depths, step height, and discharge. The location of the jump is automatically computed as part of the solution. The merit of the program to locate the jump for different initial conditions is also verified. Therefore, the model may be confidently used to design a stilling basin.

REFERENCES

1. Rouse H, Bhoota BV, Hsu EY. Design of channel expansions, high velocity flow in open channels (symposium). *Transactions* (ASCE) 1949; **116**:347–363.
2. Moore WL, Morgan CW. The hydraulic jump at an abrupt drop. *Transactions* (ASCE) 1959; **124**:507–524.
3. Ippen A, Dawson J. Design of channel contractions, high velocity flow in open channels (symposium). *Transactions* (ASCE) 1949; **116**:326–346.
4. Rajaratnam N, Ortiz NV. Hydraulic jumps and waves at abrupt drops. *Journal of Hydraulic Division* (ASCE) 1977; **103**(HY4):381–394.
5. Hager WH. B-jumps at abrupt channel drops. *Journal of Hydraulic Engineering* 1985; **111**(5):861–866.
6. Tokyay N, Gür Z. Hydraulic jump at an abrupt drop. *Doga-TR. Turkish Journal of Engineering and Environmental Sciences* 1990; **14**:215–230.
7. Ohtsu I, Yasuda Y. Transition from supercritical to subcritical flow at an abrupt drop. *Journal of Hydraulic Research* 1991; **29**(3):309–328.
8. Long D, Steffler PM, Rajaratnam N. A numerical study of submerged hydraulic jumps. *Journal of Hydraulic Research* 1991; **29**(3):293–308.
9. Gharangik AM, Chaudry MH. Numerical simulation of hydraulic jump. *Journal of Hydraulic Engineering* 1991; **117**(9):1195–1211.
10. Zhao DH, Shen HW, Lai JS, Tabios III GQ. Approximate Riemann solvers in FVM for 2D hydraulic shock wave modeling. *Journal of Hydraulic Engineering* 1996; **122**(12):692–702.
11. Zhou JG, Stansby PK. 2D shallow water flow model for the hydraulic jump. *International Journal for Numerical Methods in Fluids* 1999; **29**:375–387.
12. Stelling GS, Duinmeijer SPA. A staggered conservative scheme for every Froude number in rapidly varied shallow water flows. *International Journal for Numerical Methods in Fluids* 2003; **43**:1329–1354.
13. Mohammadian A, Le Roux DY. Simulation of shallow flows over variable topographies using unstructured grids. *International Journal for Numerical Methods in Fluids* 2006; **52**:473–498.
14. Ferreira VG, Tome MF, Mangiavacchi N, Castelo A, Cuminato JA, Fortuna AO, McKee S. High-order upwing and the hydraulic jump. *International Journal for Numerical Methods in Fluids* 2002; **39**:549–583.

DOI: 10.1002/fld

15. Stelling GS, Busnelli MM. Numerical simulation of the vertical structure of discountinuous flows. *International Journal for Numerical Methods in Fluids* 2001; **37**:23–43.
16. Lemos CM. Higher-order schemes for free surface flows with arbitrary configurations. *International Journal for Numerical Methods in Fluids* 1996; **23**:545–566.
17. Nujic M. Efficient implementation of non-oscillatory schemes for the computation of free-surface flows. *Journal of Hydraulic Research* 1995; **33**:101–111.
18. Lhomme J, Guinot V. A general approximate-state Riemann solver for hyperbolic systems of conservation laws with source terms. *International Journal for Numerical Methods in Fluids* 2007; **53**:1509–1540.
19. Caretto LS, Gosman AD, Patankar SV, Spalding DB. Two calculation procedures for steady, three-dimensional flows with recirculation. *Proceedings of the Third International Conference on Numerical Methods in Fluid Mechanics*, vol. 2. 1972; 60–68.
20. Chaudry M, Hussaini MY. Second-order accurate explicit finite difference schemes for waterhammer analysis. *Journal of Fluids Engineering* 1985; **107**:523–529.
21. Lemos CM. A simple numerical technique for turbulent flows with free surfaces. *International Journal for Numerical Methods in Fluids* 1992; **15**:127–146.
22. Bhallamudi SM, Chaudry MH. Computation of flows in open-channel transitions. *Journal of Hydraulic Research* 1992; **30**(1):77–93.
23. Garcia-Navarro P, Saviron JM. MacCormack's method for the numerical simulation of one-dimensional discontinuous unsteady open channel flow. *Journal of Hydraulic Research* 1992; **30**(1):95–105.
24. Sakarya ABA, Tokyay ND. Numerical simulation of A-type hydraulic jumps at positive steps. *Canadian Journal of Civil Engineering* 2000; **27**:805–813.
25. MacCormack RW. Numerical solution of the interaction of a shock wave with a laminar boundary layer. *Proceedings of the 2nd International Conference on Numerical Methods in Fluid Dynamics*, 15–19 September 1970, University of California, Berkeley, Holt M (ed.). Lecture Notes in Physics, vol. 8. Springer: Berlin, 1971; 151–163.
26. Gottlieb D, Turkel E. Dissipative two–four methods for time dependent problems. *Mathematics of Computation* 1976; **30**(136):703–723.
27. Chow VT. *Open-Channel Hydraulics*. McGraw-Hill: New York, 1959.
28. Chaudry MH. *Applied Hydraulic Transients*. Van Nostrand Reinhold: New York, 1987.
29. Gür Z. The hydraulic jump at an abrupt drop. *M.S. Thesis*, Civil Engineering, METU, Ankara, 1988.
30. Mingham CG, Causon DM, Ingram DM. A TVD MacCormack scheme for transcritical flow. *Proceedings ICE, Water and Maritime Engineering* 2001; **148**(3):167–175.
31. Hager WH, Bretz NV. Hydraulic jumps at positive and negative steps. *Journal of Hydraulic Research* 1986; **24**(4):237–253.

DOI: 10.1002/fld